ACS APPLIED MATERIALS & INTERFACES

www.acsami.org

Research Article

Pressure Sensor Based on a Lumpily Pyramidal Vertical Graphene Film with a Broad Sensing Range and High Sensitivity

Yifei Ma,[†] Ke Zhao,[†] Jiemin Han, Bingkang Han, Mei Wang,* Zhaomin Tong, Jonghwan Suhr, Liantuan Xiao, Suotang Jia, and Xuyuan Chen

Cite This: *ACS Appl. Mater. Interfaces* 2023, 15, 13813−13821

Read Online

ACCESS | Metrics & More | Article Recommendations | Supporting Information

ABSTRACT: Wearable sensors are vital for the development of electronic skins to improve health monitoring, robotic tactile sensing, and artificial intelligence. Active materials and the construction of microstructures in the sensitive layer are the dominating approaches to improve the performance of pressure sensors. However, it is still a challenge to simultaneously achieve a sensor with a high sensitivity and a wide detection range. In this work, using three-dimensional (3D) vertical graphene (VG) as an active material, in combination with micropyramid arrays and lumpy holders, the stress concentration effects are generated in nano-, micro-, and macroscales. Therefore, the lumpily pyramidal VG film-based pressure sensor (LPV sensor) achieves an ultrahigh sensitivity (131.36 kPa^{-1}) and a wide response range (0.1−100 kPa). Finite element analysis demonstrates that the stress concentration effects are enhanced by the micropyramid arrays and lumpy structures in micro- and macroscales, respectively. Finally, the LPV pressure sensors are tested in practical applications, including wearable health monitoring and force feedback of robotic tactile sensing.

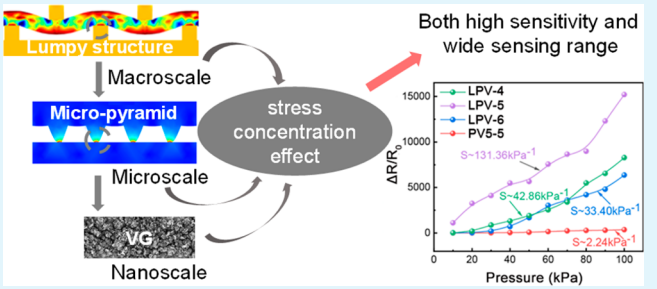

KEYWORDS: *vertical graphene, micropyramid arrays, stress concentration effect, high sensitivity, broad sensing range*

1. INTRODUCTION

With rapid development of electronic technology, intelligent devices are booming in recent years. Smartwatches, as the most representative intelligent devices, have been marketed to over 200 million last year, indicating their great popularity among consumers. Sensors are the crucial component that translates the surrounding information into electrical signals, acting as the "eyes" of intelligent devices. Most intelligent devices aim at the advantages of being portable and wearable; therefore, flexibility has become the basic requirement for sensors.[1−5] Xu et al. design a pressure sensor using flexible substrates and active materials with excellent conductivity, which has emerged for applications in wearable devices.[6] Even though many sensors already have flexible sensing hallmarks, the sensitivity and sensing range are usually incompatible. To apply to more application scenarios, maintaining high sensitivity in a wide pressure range has become a great challenge, which plays an essential role in the fields of intelligent identification and human−machine interfaces.

Active materials are determinative of the properties of the pressure sensors. Considerable amounts of active materials, such as conductive polymers,[7−10] metal nanowires,[11,12] nanoparticles,[13] silicon nanoribbons,[14] carbon black,[15] carbon nanotubes,[16−19] and graphene,[20−26] have been used in flexible sensors. Among them, graphene and its derivatives have shown great potential, owing to their superior mechanical properties and tunable microstructures. Ren et al. proposed a highly sensitive graphene-based pressure sensor to detect dynamic gait motion, which showed a sensitivity of up to 25.1 kPa^{-1} in a linearity range of 0−2.6 kPa.[27] Chen's group developed a graphene-based strain and pressure sensor, which displayed a high sensitivity of 0.36 kPa^{-1} under the pressure of 0−4 kPa and exhibited great potential in health monitoring and human motion detection.[28] In the face of significant flourish of improving sensitivity using graphene as the sensitive material, most of the sensors exhibit an appreciable sensitivity only under low pressure.[29−32] The sensitivity decreases with the increase of the pressure,[30,31,33−35] which means that the sensitivity and range of the sensor have not achieved compatibility at the same time.

Therefore, there is a great necessity to develop a high-performance flexible sensor that can effectively capitalize on the excellent properties of graphene while overcoming the limitations of existing sensors. In our previous work, the nanoscale stress concentration effect of three-dimensional

Received: January 26, 2023
Accepted: February 21, 2023
Published: March 1, 2023

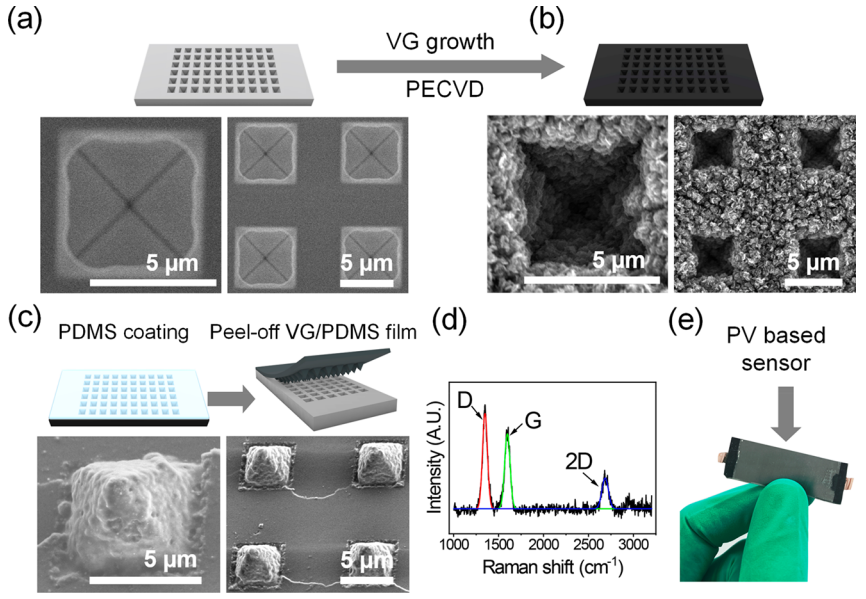

Figure 1. Schematic illustration of the fabrication process of the PV-based pressure sensor: (a) schematic illustration and top-view SEM images of the Si template with inverted micropyramid arrays prepared by photolithography, (b) schematic illustration and top-view SEM images of the pyramidal VG film on the Si template, (c) schematic illustration and top-view SEM images of convex pyramid arrays, (d) Raman spectrum of the pyramidal VG film on the Si template, and (d) photograph of a PV-based pressure sensor.

(3D) vertical graphene (VG) has been identified in a strain sensor,[36] in which the vertically aligned nanostructure renders enhanced sensing performances over the two-dimensional (2D) graphene film-based sensor. Besides active materials, a further option to broaden the sensing range and increase the sensitivity is to build a stress concentration structure in the microscale level.[37−39] However, the improvement of the sensing range still cannot satisfy the requirement. For example, Hu et al. develop a wearable pressure sensor with microstructures and achieve a sensitivity of 14.4 kPa^{-1}, while the sensing range is below 15 kPa.[40] With regard to various applications, such as robot operation and health monitoring, a high sensitivity and wide sensing range are highly required.

In this work, a lumpily pyramidal VG film-based (LPV) pressure sensor with a wide sensing range and high sensitivity is successfully achieved by introducing the stress concentration in nano-, micro-, and macroscales. The VG active layer, micropyramid arrays, and lumpy structures of the sensor provide the stress concentration effects in nano-, micro-, and macroscales, respectively, enhancing the deformation of the active layer. In this manner, the sensing range and sensitivity of the sensor are remarkably ameliorated. The relative resistance variation of the LPV-5 sensor can reach over 15 000 at 100 kPa. The finite element analysis (FEA) verifies that the micropyramid arrays and lumpy structure increase the deformation effect in micro- and macroscales of the pressure sensor. Therefore, sensors with both an outstanding sensing range and sensitivity can play a synergetic contribution in object recognition, motion monitoring, and other fields.

2. EXPERIMENTAL SECTION

2.1. Preparation of Sensors. First, a micropatterned pyramidal Si template was fabricated as the substrate for VG growth. The pyramid pattern was defined by photography on a 4 in. Si wafer, and then silicon was etched chemically and anisotropically using potassium hydroxide. Each pyramid had a square area of 5 × 5 μm. The micropatterned Si mold was cleaned with alcohol and acetone with ultrasonication. The Si template was put into a tubular furnace for VG growth using a plasma-enhanced chemical vapor deposition (PECVD) process. The furnace was heated to 900 °C at a pressure lower than 1 mTorr. H_2 [2 standard cubic centimeters per minute (sccm)] and C_2H_2 (6 sccm) flowed into the furnace, and VG was grown at a plasma power of 500 W for 1 h, followed by natural cooling to room temperature. As a result, the VG film was grown on the mold surface with a thickness of around 5 μm. A Dow Corning Sylgard 184 silicone elastomer was mixed at the ratio of 13:1 to prepare the polydimethylsiloxane (PDMS) solution. Then, the PDMS solution was poured onto the mold surface, and a film with 600 μm in thickness was formed. Afterward, the VG/PDMS film can be peeled off from the mold after curing at 80 °C for 2 h. By this means, the pyramidal VG arrays were successfully attached to the PDMS surface, serving as the active layer of the pressure sensor. The pyramidal VG film (PV)-based sensors are named according to the size and intervals of the pyramids (Figure S1 of the Supporting Information), in which the first number indicates the pyramid size and the second number represents the interval between pyramids (Table S1 of the Supporting Information). For example, the sensor with 5 μm pyramid size and 5 μm pyramid interval is denoted as PV5-5. The sensor based on a flat VG film without patterns is named flat VG. Because silicon ⟨100⟩ was etched at a fixed angle (54.74°), the height of pyramids can be calculated by the size of the pyramid. As illustrated in Figure S2 of the Supporting Information, the heights of the pyramids with sizes of 5, 10, 20, and 50 μm are 3.54, 7.07, 14.14, and 35.36 μm.

A HORI 3D printer (E2) is utilized to fabricate the auxiliary deformation holders using polylactic acid (PLA) filament. The operation temperature of the printer was 210 °C, and the printing speed was set to 40 mm/s. The upper holder consisted of four stripes with an interval, height, and width of 5, 1, and 1 mm, respectively. The lower holder was composed of five stripes with an interval, height, and width of 5, 1, and 1 mm, respectively. The sensor was assembled in a sandwich structure with the VG/PDMS film placed between the upper and lower holders. The resulting LPV-based sensors with intervals of 4, 5, and 6 mm are named LPV-4, LPV-5, and LPV-6, respectively. For comparison, the sensor based on lumpy flat VG with a grid interval of 5 mm is also prepared, which is named LFV-5.

To exhibit the superior property of VG, two-dimensional (2D) graphene was also synthesized as the active layer of the pressure sensor as a control group. The Si wafer was used as the growth

https://doi.org/10.1021/acsami.3c01175
ACS Appl. Mater. Interfaces 2023, 15, 13813−13821

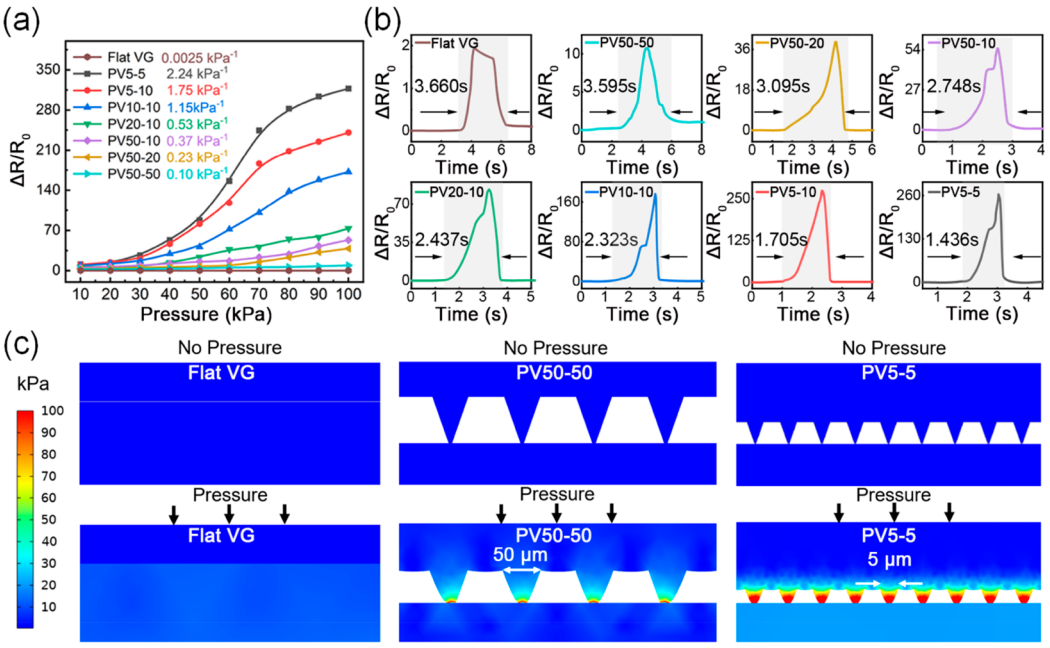

Figure 2. (a) Relative resistance changes of the flat VG- and PV-based sensors at the pressure of 10−100 kPa, (b) resistance response of the PV-based sensors with different sizes and intervals of micropyramid arrays under the pressure of 100 kPa, and (c) finite element analysis of the pressure distribution on the flat VG-based sensor, PV50-50, and PV5-5.

substrate and put into the tubular furnace. The furnace was heated to 900 °C at a pressure lower than 1 mTorr. Then, 6 sccm of C_2H_2 and 2 sccm of H_2 flowed into the furnace for 30 s under the plasma power of 500 W. The sensor based on 2D graphene is named flat Gr. The pyramidal 2D graphene sensor with a pyramid size and interval of 5 μm is denoted as PG5-5, and lumpily pyramidal 2D graphene with a pyramid size and interval of 5 μm and grid interval of 5 mm is named LPG-5. Detailed conditions of all fabricated sensors are shown in Table S1 of the Supporting Information.

2.2. Characterization and Measurements. Scanning electron microscopy (SEM, Hitachi SU-8010) was used to characterize the morphology of the samples. Raman spectra were recorded on a Horiba Scientific LabRAM HR Evolution Raman microscope with a laser operated at 523 nm. The pressure was applied by an electric tensile pressure tester (ZQ-990B). Resistance was recorded by a Keysight E4980A Precision LCR meter.

2.3. Sensitivity. Sensitivity is a key parameter to evaluate the sensing performance of pressure sensors. Sensitivity is defined as $S = (\Delta R/R_0)/\Delta P$, where ΔR is the resistance change before and after pressure is applied, R_0 is the initial resistance, and ΔP is the pressure change.

2.4. Pressure. The pressure is calculated by the formula $P = F/A$, where F is the force applied by the electric tensile pressure tester and A is the area of the sensor. The sensor is 4 cm long and 1.5 cm wide. The area of the sensor works out to 6 cm^2.

2.5. FEA Simulation. *2.5.1. Simulation of the Pressure Distribution on the Flat VG-Based Sensor, PV50-50, and PV5-5.* FEA is implemented using COMSOL Multiphysics 5.6. The pyramids with a width of 5 μm and height of $20/\pi$ μm were carried out in the analysis. In the simulation model, the boundary road of 10 kPa was applied on the surface. The tip of the pyramid would be pressed against the hard surface to deform. The model is analyzed by a physical model of plane strain under 2D approximation.

2.5.2. Simulation of the LPV Sensor in the Macroscale. The total length of the model was set as 25 mm in the simulation, and the intervals of the holders were 4, 5, and 6 mm, respectively. In the simulation model, 100 kPa of pressure was applied to the upper surface.

2.5.3. Simulation of the Pressure Distribution of 2D Graphene and VG. In the 2D approximation, a triangle with a base length of 5 μm and height of 3.5 μm was designed to simulate a single pyramid. VG layers were vertically distributed on the edge of the pyramid, and 2D graphene was attached to the edge of the pyramid. Pressure distributions of VG and 2D graphene on the micropyramid at 10 kPa were simulated.

3. RESULTS AND DISCUSSION

The schematic illustration of the fabrication process of the PV-based pressure sensor is presented in Figure 1. VG was grown on an inverted micropyramid array patterned silicon wafer by the PECVD method. After the growth process, the surface of silicon was fully covered with vertically oriented graphene sheets (Figure 1b). The successful growth of VG is also confirmed by the Raman spectrum (Figure 1d), in which representative D, G, and 2D peaks appear at 1350, 1608, and 2680 cm^{-1}. Afterward, PDMS was spin-coated followed by peeling off VG from the substrate to obtain the VG/PDMS film, in which the convex pyramid arrays were constructed, as presented in Figure 1c. VG is composed of a planar carbon layer and vertically oriented graphene sheets (Figure S3 of the Supporting Information). When pressure is applied, VG may provide stress concentration effects in the nanoscale level, and the pyramidal structure is beneficial to provide the stress concentration in the microscale level. By attachment of two electrodes, the flexible pressure sensor based on the pyramidal VG film is obtained, as shown in Figure 1e.

To investigate the dynamic piezoresistive response to the pressure, the PV-based sensor is connected to a digital LCR meter and loaded onto a tensile pressure testing machine, as shown in Figure S4 of the Supporting Information. The sensing performance is illustrated in Figure 2. The PV-based sensors with different sizes and intervals of the pyramid array were tested, while flat VG/PDMS without a pyramid array was also tested as a control. As shown in Figure 2a and Figures S5−S12 of the Supporting Information, the relative resistance changes ($\Delta R/R_0$) of the PV-based sensors under a series of pressures are depicted, from which the sensitivities of the PV-based sensors with different pyramid structures are calculated.

https://doi.org/10.1021/acsami.3c01175
ACS Appl. Mater. Interfaces 2023, 15, 13813−13821

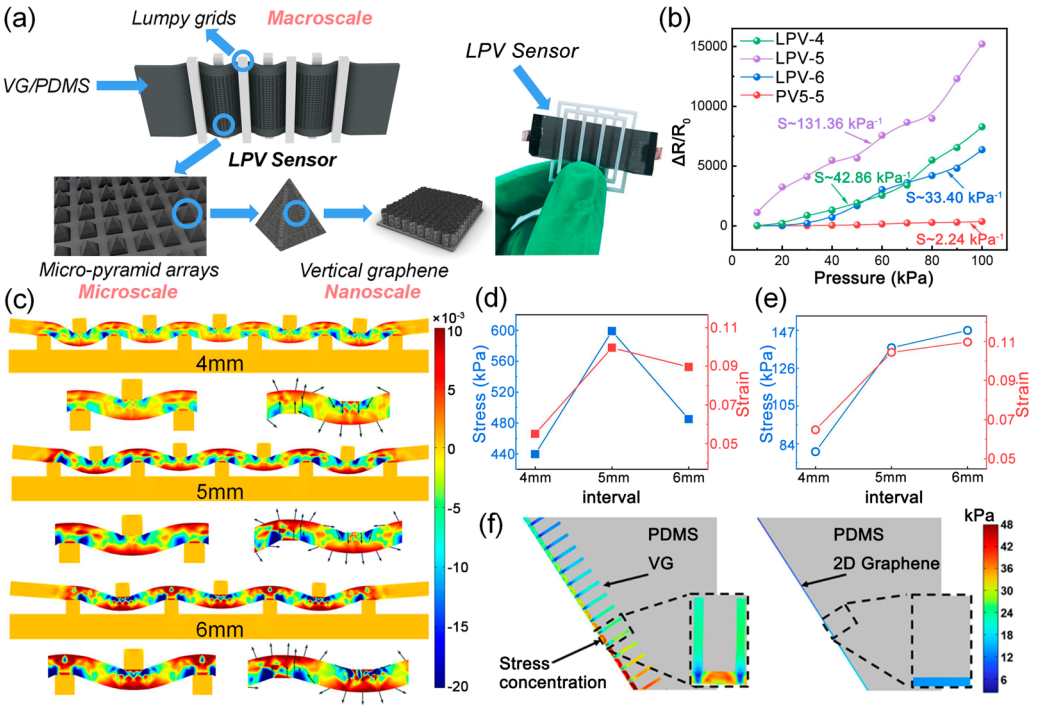

Figure 3. (a) Schematic illustration and a digital photograph of a lumpily pyramidal VG film-based pressure sensor (LPV sensor), (b) comparison in resistance change of LPV-4, LPV-5, LPV-6, and PV5-5, (c) corresponding finite element analysis of the stress concentration of LPV-4, LPV-5, and LPV-6, (d) simulation results of whole-unit stress and strain results of the LPV sensors, (e) simulation results of single-unit stress and simulation results of the LPV sensors, and (f) simulation of the pressure distribution of VG and 2D graphene.

The flat VG sensor shows the lowest sensitivity of 0.0025 kPa^{-1}, demonstrating that the pyramid structures obviously enhance the sensitivity of the PV-based sensors. In addition, the sensitivity is closely related to the profiles of the pyramid arrays. When the size of the pyramid is fixed, the sensitivities are increasing with the decrease of the intervals between pyramids. Furthermore, the sensitivities are increasing with the decreased size of the pyramids under a fixed pyramid interval. Therefore, higher sensitivity can be achieved with a larger interval and a smaller size of pyramids. Hence, the PV5-5-based sensor achieves the highest sensitivity of 2.24 kPa^{-1} with a large response limit of up to 100 kPa. As a result, the micropyramid VG array can prominently improve the sensing performances of the VG-based sensors in the microscale level.

The response time of the PV-based sensors was tested under the pressure of 100 kPa. As depicted in Figure 2b, the pyramid structure obviously improves the piezoresistive response of the sensors. PV5-5 with the micropyramids and intervals provides the largest $\Delta R/R_0$ (263.7), which is 136.6 times higher than that of the flat VG-based sensor and 24.5 times higher than that of PV50-50. In comparison to the PV-based sensors, the flat VG-based sensor shows the longest response time of 3.660 s; meanwhile, a recovering time of 2 s is also observed. Fast recovery is obtained by the PV-based sensors when releasing the pressure. The response time shortens with the decrease of the size and intervals of the pyramids. As a result, the PV5-5 sensor exhibits the shortest response time of 1.436 s under the pressure of 100 kPa, which is 2.5 times faster than the flat VG-based sensor, greatly improving the sensing performance at a high pressure. It is demonstrated that the PV-based sensors possess high sensitivity and fast response in a broad range, and the sensing properties are improved with the decrease of size and intervals of the pyramids.

A distinguishable improvement has been achieved by constructing the pyramidal structure in the microscale level. To clarify the advantages of the pyramidal microstructure, finite element analysis is employed to simulate the deformation of micropyramid structures under pressure, as shown in Figure 2c. Undoubtedly, the flat structure uniformly distributes the pressure, and no stress concentration is observed. On the contrary, for the PV-based sensor, the tips of pyramids will first be compressed when pressing, leading to a concentrated stress that greatly deforms VG on the tips in the microscale level. As a result, the resistance of the micropyramid-based sensors increases significantly. Furthermore, with the decrease of the size of pyramids from 50 to 5 μm, the stress concentration effect is further enhanced in the microscale level. In addition, a short interval will augment the number of pyramids per unit area and increase the density of stress concentration points, thus further improving the sensitivity of the sensor. Hence, the PV-based sensor with a smaller pyramid and shorter interval will possess better sensing performances, which is perfectly in accordance with the experimental results.

In the microscale level, as demonstrated above, the micropyramid arrays offer a distinguishable stress concentration effect. To further optimize the sensing performance, a 3D-printed frame in the macroscale is designed as a holder on both sides of the PV-based sensor to provide more stress concentration sites and increase the deformation effect, as shown in Figure 3a. In this strategy, we designed a lumpily pyramidal VG film-based pressure sensor (LPV sensor), in which the VG/PDMS film crimps along the grids under pressure. All of the PV films for the subsequent characterizations are PV5-5. As a result, as shown in panels b and c of Figure 3, the direction of the vertically downward force along the grids is changed, resulting in a horizontal component that

https://doi.org/10.1021/acsami.3c01175
ACS Appl. Mater. Interfaces 2023, 15, 13813−13821

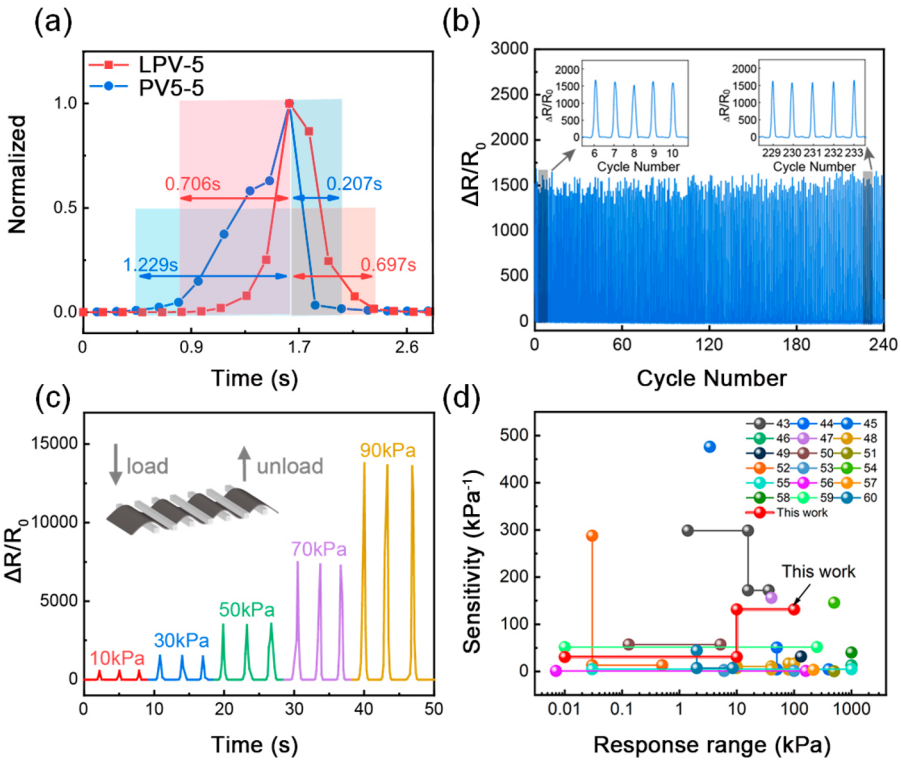

Figure 4. (a) Response and recovery time of LPV-5, (b) durability of LPV-5 under a loading pressure of 30 kPa, (c) resistance response of LPV-5 under various pressures of 10, 30, 50, 70, and 90 kPa, and (d) comparison of the response range and sensitivity of LPV-5 with reported pressure sensors.

causes tensile force along the sensor (Figure 3c), thereby enhancing the resistance variation in the macroscale (Figure 3b). The grids are carefully designed with intervals of 4, 5, and 6 mm, respectively. The simulation results show that the stress and strain on each grid are increasing with the increase of grid intervals (Figure 3c). In addition, the total length of the grid holder should match the LPV sensor. In terms of this study, the LPV sensor can match 5 units of the grid with intervals of 4 mm, 4 units of the grid with intervals of 5 mm, or 3 units of the grid with intervals of 6 mm. According to the results of the simulation, LPV-5 has the highest total stress and strain of 598.90 kPa and 9.71% (Figure 3d), respectively. The experimental results also confirm that a tremendous boost to the sensitivity of the LPV sensor is obtained with the help of grids, as shown in Figure 3b. Meanwhile, LPV-5 shows the highest sensitivity of 131.36 kPa^{-1}, which is 58.6 times higher than that of the PV-based sensor (without grid), 3.1 times higher than that of LPV-4, and 2.6 times higher than that of LPV-6, as shown in Figure 3e. Moreover, the sensor based on lumpy flat VG with a grid interval of 5 mm (LFV-5) is fabricated to investigate the effect of the structure design in micro- and macroscales (Figure S13 of the Supporting Information). By the macroscale structure design, the sensitivity of LFV-5 improved ~25 times over that of flat VG, while it is still far away from the application requirement. As shown in Table S2 of the Supporting Information, the sensitivity enhancement by the macroscale lumpy structure (LFV-5, 25 times) is much less than that by the microscale pyramid structure (PV5-5, 896 times). These results demonstrate that the greatest advance of the VG-based sensor can be achieved by the combination of the microscale pyramid structure and macroscale lumpy structure (LPV-5, 52 544 times).

In addition, as illustrated in Figures S14 and S15 of the Supporting Information, the LPV-5 sensor exhibits a superior response to LPV-4 and LPV-6, at the low-pressure range of 0.1−10 kPa. The sensor has a remarkable sensitivity over the entire pressure range below 100 kPa, especially in the range of 10−100 kPa (Figure S14 of the Supporting Information). It is worth noting that LPV-5 can detect the lowest limit of 100 Pa. Consequently, through the effect of VG on the nanoscale level, micropyramid arrays on the microscale level and lumpy structures on the macroscale level, the synergistic effects of the stress concentration strategies are developed, achieving an excellent sensitivity in a broad pressure range of 0.1−100 kPa.

To investigate the sensing mechanism of VG, the FEA was implemented to reveal the sensing priority of 3D VG over 2D graphene. Figure 3f shows the FEA simulation of the pressure distribution of VG and 2D graphene under the same applied pressure. VG is composed of vertically aligned VG flakes and a planar carbon buffer layer (panels c and f of Figure 1).[41,42] The vertically aligned graphene nanoflakes embed in PDMS and grasp PDMS like tree roots, and thus, the heterotypic structure causes the heterogeneous pressure distribution. The pressure mainly concentrates on the valley of VG, that is, the buffer layer of VG, which directly determines the resistance of VG. However, the pressure distributed on 2D graphene gradually varies from the pyramid tip to bottom, and the average pressure is 2.76 times lower than that on VG. Experimental characterization results of the 2D graphene-based sensors in Figure S16 of the Supporting Information confirm that the VG-based sensors possess superior resistance response to the

https://doi.org/10.1021/acsami.3c01175
ACS Appl. Mater. Interfaces 2023, 15, 13813−13821

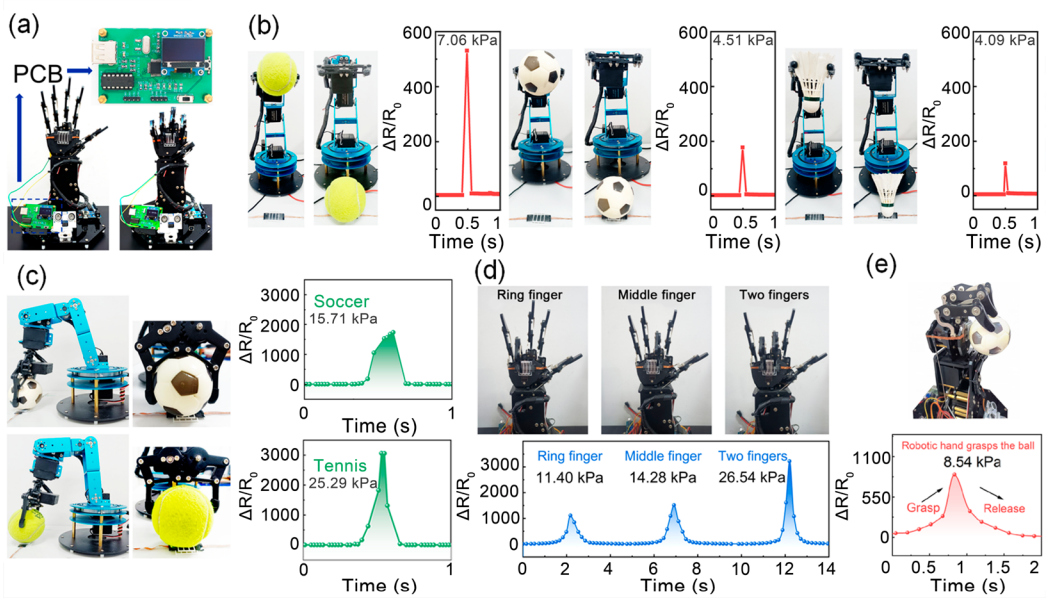

Figure 5. (a) Photograph of the pressure sensing system to detect the pressure on the palm of the robotic hand using LPV-5, (b) sensing system to detect the pressure when different objects fall onto LPV-5, (c) pressure sensing with a robotic arm catching a soft soccer ball and a hard tennis ball to press on LPV-5, (d) Attachment of LPV-5 on a robotic hand using different fingers to press the sensor, and (e) pressure sensing for a robotic hand grasping a soft soccer ball.

pressure, demonstrating the important role of the nanoscale structure design.

According to the above experimental and theoretical results, the sensing mechanism of the LPV sensors is summarized. Basically, the piezoresistive sensor is based on the principle of resistance variation of the conductive layer caused by the material deformation under the external force (pressure). In LPV, a scrupulous structure design is implemented on the conductive graphene layer in nano-, micro-, and macroscales (Figure 3a). In the nanoscale, VG with vertically orientated nanostructures provides the stress concentration on the valley of VG nanoflakes, enhancing the resistance variation under the external pressure (Figure 3f and Figure S16 of the Supporting Information). In the microscale, the pyramid arrays greatly strengthen the stress concentration on the pyramid tips, amplifying the resistance variation of VG (Figure 2c). In the macroscale, the grid holders are used to construct a lumpy structure of VG/PDMS, contributing to the deformation of VG on the crest and trough regions (Figure 3c) and further enhancing the resistance variation. As a result, the preeminent sensing performances of the LPV sensors are attributed to a synergistic effect of the nano-, micro-, and macrostructure designs of VG.

Response time characterization is conducted on LPV-5 under the pressure of 100 kPa. As shown in Figure 4a, the grid helps shorten the response time, while the sensor with the grid holders requires a longer recovering time compared to the sensor without a grid. The total response time is almost the same. In addition, the repeatability of a sensor is important for practical applications. The repeatability test was performed on LPV-5 under a loading pressure of 30 kPa. As depicted in the insets of Figure 4b, a distinct increase of $\Delta R/R_0$ is observed, showing a sharp rectangular signal. Impressively, LPV-5 exhibits a stable response to the pressure. The response of LPV-5 in the initial cycles is almost the same as the last cycles, indicating the excellent durability of the LPV sensor. Furthermore, we also tested the real-time response of the sensor with cyclic loading under pressures of 10, 30, 50, 70, and 90 kPa for 3 cycles per pressure (Figure 4c). The results show that LPV-5 presents stable responses with excellent repeatability. Figure 4d shows a high sensitivity response over a wide response range compared to reported pressure sensors, demonstrating the supereminent sensing properties of our LPV-5 sensor.[43−60]

The practical application is important to characterize the performance of the sensor. Herein, a printed circuit board (PCB) is designed for LPV-5 to transform resistance signals to pressure, which is displayed on the small screen (Figure 5a). The circuit diagram and working principle are shown in Figure S17 of the Supporting Information. As shown in Figure 5b, LPV-5 is attached to a table to detect the impacts of falling objects (Movies S1−S3 of the Supporting Information). A tennis ball, a toy soccer ball, and a badminton shuttlecock are dropped from the same height. Owing to the different weights and shapes, the falling tennis ball causes an impact pressure of 7.06 kPa, while the relatively light toy soccer ball and badminton shuttlecock cause weaker impacts of 4.51 and 4.09 kPa, respectively. Then, the robotic arm holds the toy soccer ball and the hard tennis ball to press LPV-5 in the same position (Movies S4 and S5 of the Supporting Information). Because the toy soccer ball is made from rubber, it will deform during the test, thereby abasing the pressure loading on LPV-5. Therefore, pushing with a soft toy soccer ball causes a lower pressure of 15.71 kPa than that of 25.29 kPa with a hard tennis ball (Figure 5c).

In terms of biomimetic machines, the pressure sensor is particularly important to monitor the surroundings and provide feedback during operation. Therefore, LPV-5 is attached to the center of the palm of a robotic hand to detect the pressure applied to it (Figure 5d). When the fingers are bent, the ring and middle fingers will exert pressures of 11.40 and 14.28 kPa, respectively. A pressure of 26.54 kPa is obtained when two fingers push LPV-5 together. When grabbing, the pressure that is put on the target object can be

https://doi.org/10.1021/acsami.3c01175
ACS Appl. Mater. Interfaces 2023, 15, 13813−13821

reflected from LPV-5. As shown in Figure 5e, the robotic hand grasps a toy soccer ball and exerts a pressure of 8.54 kPa. Hence, the LPV sensor shows great promise in the grasp force feedback of the robots for adapting the grasping behavior under various application scenarios.

4. CONCLUSION

In summary, a lumpily pyramidal vertical graphene film-based pressure sensor with both a high sensitivity and broad sensing range was designed and fabricated. In comparison to the typical flat VG film sensor, the micropyramid arrays and lumpy structure of the sensor strongly enhance the stress concentration effect in micro- and macroscales, respectively. By virtue of the nanoscale stress concentration effect of VG, the stress concentration effects are devoted to the LPV sensor in nano-, micro-, and macroscales. Therefore, LPV-5 exhibits a remarkable sensitivity of 131.36 kPa^{-1} and a wide detection range of 0.1−100 kPa, achieving a high sensitivity over a wide sensing range. Finally, the facile fabrication, high sensitivity, and wide sensing range of the LPV sensor make it a promising candidate in the fields of object recognition and human−machine interfaces.

■ ASSOCIATED CONTENT

Supporting Information

The Supporting Information is available free of charge at https://pubs.acs.org/doi/10.1021/acsami.3c01175.

Illustration of the size and interval of the pyramids in the PV-based sensors (Figure S1), schematic illustration of the anisotropic wet etching process of silicon (Figure S2), cross-sectional SEM image of VG (Figure S3), pressure testing system (Figure S4), resistance response of the PV5-5, PV5-10, PV10-10, PV20-10, PV50-10, PV50-20, PV50-50, and flat VG sensors under the pressure range of 10−100 kPa (Figures S5−S12), resistance response of the flat VG and LFV-5 sensors (Figure S13), resistance response of the LPV-5 sensor at (a) 100−1000 Pa, (b) 1−10 kPa, and (c) 10−100 kPa and resistance response variation curves of the LPV-5 sensor at (d) 100−1000 Pa, (e) 1−10 kPa, and (f) 10−100 kPa (Figure S14), relative resistance changes of the LPV-4 sensor at (a) 0.1−1 kPa and (b) 1−10 kPa and relative resistance changes of the LPV-6 sensor at (c) 0.1−1 kPa and (d) 1−10 kPa (Figure S15), comparison of the resistance response of the flat Gr, flat VG, PG5-5, and LPG-5 sensors (Figure S16), circuit diagram of the pressure sensing system (Figure S17), detailed conditions of sensors (Table S1), and comparison of the VG-based sensor in different scale effects (Table S2) (PDF)

Sensing system to detect the pressure when a badminton shuttlecock falls onto LPV-5 (Movie S1) (MP4)

Sensing system to detect the pressure when a toy soccer ball falls onto LPV-5 (Movie S2) (MP4)

Sensing system to detect the pressure when a tennis ball falls onto LPV-5 (Movie S3) (MP4)

Pressure sensing with a robotic arm catching a soft soccer ball to press on LPV-5 (Movie S4) (MP4)

Pressure sensing with a robotic arm catching a hard tennis ball to press on LPV-5 (Movie S5) (MP4)

■ AUTHOR INFORMATION

Corresponding Author

Mei Wang − *State Key Laboratory of Quantum Optics and Quantum Optics Devices, Institute of Laser Spectroscopy, Collaborative Innovation Center of Extreme Optics, Shanxi University, Taiyuan, Shanxi 030006, People's Republic of China;* orcid.org/0000-0003-4127-4983; Email: wangmei@sxu.edu.cn

Authors

Yifei Ma − *State Key Laboratory of Quantum Optics and Quantum Optics Devices, Institute of Laser Spectroscopy, Collaborative Innovation Center of Extreme Optics, Shanxi University, Taiyuan, Shanxi 030006, People's Republic of China*

Ke Zhao − *State Key Laboratory of Quantum Optics and Quantum Optics Devices, Institute of Laser Spectroscopy, Collaborative Innovation Center of Extreme Optics, Shanxi University, Taiyuan, Shanxi 030006, People's Republic of China*

Jiemin Han − *State Key Laboratory of Quantum Optics and Quantum Optics Devices, Institute of Laser Spectroscopy, Collaborative Innovation Center of Extreme Optics, Shanxi University, Taiyuan, Shanxi 030006, People's Republic of China*

Bingkang Han − *State Key Laboratory of Quantum Optics and Quantum Optics Devices, Institute of Laser Spectroscopy, Collaborative Innovation Center of Extreme Optics, Shanxi University, Taiyuan, Shanxi 030006, People's Republic of China*

Zhaomin Tong − *State Key Laboratory of Quantum Optics and Quantum Optics Devices, Institute of Laser Spectroscopy, Collaborative Innovation Center of Extreme Optics, Shanxi University, Taiyuan, Shanxi 030006, People's Republic of China*

Jonghwan Suhr − *Department of Polymer Science and Engineering, School of Mechanical Engineering, Sungkyunkwan University, Suwon, Gyeonggi 16419, Republic of Korea;* orcid.org/0000-0003-3491-5738

Liantuan Xiao − *State Key Laboratory of Quantum Optics and Quantum Optics Devices, Institute of Laser Spectroscopy, Collaborative Innovation Center of Extreme Optics, Shanxi University, Taiyuan, Shanxi 030006, People's Republic of China*

Suotang Jia − *State Key Laboratory of Quantum Optics and Quantum Optics Devices, Institute of Laser Spectroscopy, Collaborative Innovation Center of Extreme Optics, Shanxi University, Taiyuan, Shanxi 030006, People's Republic of China*

Xuyuan Chen − *State Key Laboratory of Quantum Optics and Quantum Optics Devices, Institute of Laser Spectroscopy, Collaborative Innovation Center of Extreme Optics, Shanxi University, Taiyuan, Shanxi 030006, People's Republic of China; Faculty of Technology, Natural Sciences and Maritime Sciences, Department of Microsystems, University of South-Eastern Norway, N-3184 Borre, Norway*

Complete contact information is available at: https://pubs.acs.org/10.1021/acsami.3c01175

Author Contributions

†Yifei Ma and Ke Zhao contributed equally to this work.

Notes

The authors declare no competing financial interest.

■ ACKNOWLEDGMENTS

This research was supported by the National Key Research and Development Program of China (Grant 2022YFA1404001), the National Natural Science Foundation of China (Grants 21805174 and 51902190), the Key Research and Development Program of Shanxi Province for International Cooperation (201803D421082), the Research Project supported by Shanxi Scholarship Council of China (2021-004 and 2022-013), the 111 Project (Grant D18001), the Changjiang Scholars and Innovative Research Team in University of Ministry of Education of China (Grant IRT_17R70), and the Fund for Shanxi "1331 Project".

■ REFERENCES

(1) Park, S.; Vosguerichian, M.; Bao, Z. A Review of Fabrication and Applications of Carbon Nanotube Film-Based Flexible Electronics. *Nanoscale* **2013**, *5* (5), 1727−1752.
(2) Liu, Y.; Wang, H.; Zhao, W.; Zhang, M.; Qin, H.; Xie, Y. Flexible, Stretchable Sensors for Wearable Health Monitoring: Sensing Mechanisms, Materials, Fabrication Strategies and Features. *Sensors* **2018**, *18* (2), 645.
(3) Jayathilaka, W.; Qi, K.; Qin, Y.; Chinnappan, A.; Serrano-Garcia, W.; Baskar, C.; Wang, H.; He, J.; Cui, S.; Thomas, S. W.; Ramakrishna, S. Significance of Nanomaterials in Wearables: A Review on Wearable Actuators and Sensors. *Adv. Mater.* **2019**, *31* (7), 1805921.
(4) Xu, K.; Lu, Y.; Takei, K. Multifunctional Skin-Inspired Flexible Sensor Systems for Wearable Electronics. *Adv. Mater. Technol.* **2019**, *4* (3), 1800628.
(5) Lou, Z.; Wang, L.; Jiang, K.; Wei, Z.; Shen, G. Reviews of Wearable Healthcare Systems: Materials, Devices And System Integration. *Mater. Sci. Eng., R* **2020**, *140*, 100523.
(6) Chen, S.; Song, Y.; Xu, F. Flexible and Highly Sensitive Resistive Pressure Sensor Based on Carbonized Crepe Paper with Corrugated Structure. *ACS Appl. Mater. Interfaces* **2018**, *10* (40), 34646−34654.
(7) Hu, N.; Karube, Y.; Yan, C.; Masuda, Z.; Fukunaga, H. Tunneling Effect in a Polymer/Carbon Nanotube Nanocomposite Strain Sensor. *Acta Mater.* **2008**, *56* (13), 2929−2936.
(8) Choong, C. L.; Shim, M. B.; Lee, B. S.; Jeon, S.; Ko, D. S.; Kang, T. H.; Bae, J.; Lee, S. H.; Byun, K. E.; Im, J.; Jeong, Y. J.; Park, C. E.; Park, J. J.; Chung, U. I. Highly Stretchable Resistive Pressure Sensors Using a Conductive Elastomeric Composite on a Micropyramid Array. *Adv. Mater.* **2014**, *26* (21), 3451−3458.
(9) Pan, L.; Chortos, A.; Yu, G.; Wang, Y.; Isaacson, S.; Allen, R.; Shi, Y.; Dauskardt, R.; Bao, Z. An Ultra-Sensitive Resistive Pressure Sensor Based on Hollow-Sphere Microstructure Induced Elasticity in Conducting Polymer Film. *Nat. Commun.* **2014**, *5*, 3002.
(10) Yao, S.; Zhu, Y. Wearable Multifunctional Sensors Using Printed Stretchable Conductors Made of Silver Nanowires. *Nanoscale* **2014**, *6* (4), 2345−2352.
(11) Amjadi, M.; Pichitpajongkit, A.; Lee, S.; Ryu, S.; Park, I. Highly Stretchable and Sensitive Strain Sensor Based on Silver Nanowire-Elastomer Nanocomposite. *ACS Nano* **2014**, *8* (5), 5154−5163.
(12) Hwang, B. U.; Lee, J. H.; Trung, T. Q.; Roh, E.; Kim, D. I.; Kim, S. W.; Lee, N. E. Transparent Stretchable Self-Powered Patchable Sensor Platform with Ultrasensitive Recognition of Human Activities. *ACS Nano* **2015**, *9* (9), 8801−8810.
(13) Segev-Bar, M.; Haick, H. Flexible Sensors Based on Nanoparticles. *ACS Nano* **2013**, *7* (10), 8366−8378.
(14) Han, X. G.; Funk, M. R.; Shen, F.; Chen, Y. C.; Li, Y. Y.; Campbell, C. J.; Dai, J. Q.; Yang, X. F.; Kim, J. W.; Liao, Y. L.; Connell, J. W.; Barone, V.; Chen, Z. F.; Lin, Y.; Hu, L. B. Scalable Holey Graphene Synthesis and Dense Electrode Fabrication toward High-Performance Ultracapacitors. *ACS Nano* **2014**, *8* (8), 8255−8265.
(15) Lu, N.; Lu, C.; Yang, S.; Rogers, J. Highly Sensitive Skin-Mountable Strain Gauges Based Entirely on Elastomers. *Adv. Funct. Mater.* **2012**, *22* (19), 4044−4050.
(16) Yamada, T.; Hayamizu, Y.; Yamamoto, Y.; Yomogida, Y.; Izadi-Najafabadi, A.; Futaba, D. N.; Hata, K. A Stretchable Carbon Nanotube Strain Sensor for Human-Motion Detection. *Nat. Nanotechnol.* **2011**, *6* (5), 296−301.
(17) Park, J.; Lee, Y.; Hong, J.; Lee, Y.; Ha, M.; Jung, Y.; Lim, H.; Kim, S. Y.; Ko, H. Tactile-Direction-Sensitive and Stretchable Electronic Skins Based on Human-Skin-Inspired Interlocked Microstructures. *ACS Nano* **2014**, *8* (12), 12020−12029.
(18) Liu, Z.; Qi, D.; Guo, P.; Liu, Y.; Zhu, B.; Yang, H.; Liu, Y.; Li, B.; Zhang, C.; Yu, J.; Liedberg, B.; Chen, X. Thickness-Gradient Films for High Gauge Factor Stretchable Strain Sensors. *Adv. Mater.* **2015**, *27* (40), 6230−6237.
(19) Ryu, S.; Lee, P.; Chou, J. B.; Xu, R. Z.; Zhao, R.; Hart, A. J.; Kim, S. G. Extremely Elastic Wearable Carbon Nanotube Fiber Strain Sensor for Monitoring of Human Motion. *ACS Nano* **2015**, *9* (6), 5929−5936.
(20) Lin, Y.; Liu, S.; Chen, S.; Wei, Y.; Dong, X.; Liu, L. A Highly Stretchable and Sensitive Strain Sensor Based on Graphene−Elastomer Composites with a Novel Double-Interconnected Network. *J. Mater. Chem. C* **2016**, *4* (26), 6345−6352.
(21) Yan, C.; Wang, J.; Kang, W.; Cui, M.; Wang, X.; Foo, C. Y.; Chee, K. J.; Lee, P. S. Highly Stretchable Piezoresistive Graphene-Nanocellulose Nanopaper for Strain Sensors. *Adv. Mater.* **2014**, *26* (13), 2022−2027.
(22) Hempel, M.; Nezich, D.; Kong, J.; Hofmann, M. A Novel Class of Strain Gauges Based on Layered Percolative Films of 2D Materials. *Nano Lett.* **2012**, *12* (11), 5714−5718.
(23) Boland, C. S.; Khan, U.; Backes, C.; O'Neill, A.; McCauley, J.; Duane, S.; Shanker, R.; Liu, Y.; Jurewicz, I.; Dalton, A. B.; Coleman, J. N. Sensitive, High-Strain, High-Rate Bodily Motion Sensors Based on Graphene-Rubber Composites. *ACS Nano* **2014**, *8* (9), 8819−8830.
(24) Cheng, Y.; Wang, R.; Sun, J.; Gao, L. A Stretchable and Highly Sensitive Graphene-Based Fiber for Sensing Tensile Strain, Bending, and Torsion. *Adv. Mater.* **2015**, *27* (45), 7365−7371.
(25) Wang, Y.; Yang, R.; Shi, Z. W.; Zhang, L. C.; Shi, D. X.; Wang, E.; Zhang, G. Y. Super-Elastic Graphene Ripples for Flexible Strain Sensors. *ACS Nano* **2011**, *5* (5), 3645−3650.
(26) Zhao, J.; Wang, G. L.; Yang, R.; Lu, X. B.; Cheng, M.; He, C. L.; Xie, G. B.; Meng, J. L.; Shi, D. X.; Zhang, G. Y. Tunable Piezoresistivity of Nanographene Films for Strain Sensing. *ACS Nano* **2015**, *9* (2), 1622−1629.
(27) Tao, L. Q.; Zhang, K. N.; Tian, H.; Liu, Y.; Wang, D. Y.; Chen, Y. Q.; Yang, Y.; Ren, T. L. Graphene-Paper Pressure Sensor for Detecting Human Motions. *ACS Nano* **2017**, *11* (9), 8790−8795.
(28) Yang, J. Y.; Ye, Y. S.; Li, X. P.; Lu, X. Z.; Chen, R. J. Flexible, Conductive, and Highly Pressure-Sensitive Graphene-Polyimide Foam for Pressure Sensor Application. *Compos. Sci. Technol.* **2018**, *164*, 187−194.
(29) Pang, Y.; Zhang, K. N.; Yang, Z.; Jiang, S.; Ju, Z. Y.; Li, Y. X.; Wang, X. F.; Wang, D. Y.; Jian, M. Q.; Zhang, Y. Y.; Liang, R. R.; Tian, H.; Yang, Y.; Ren, T. L. Epidermis Microstructure Inspired Graphene Pressure Sensor with Random Distributed Spinosum for High Sensitivity and Large Linearity. *ACS Nano* **2018**, *12* (3), 2346−2354.
(30) Chang, T. H.; Tian, Y.; Li, C.; Gu, X.; Li, K.; Yang, H.; Sanghani, P.; Lim, C. M.; Ren, H.; Chen, P. Y. Stretchable Graphene Pressure Sensors with Shar-Pei-like Hierarchical Wrinkles for Collision-Aware Surgical Robotics. *ACS Appl. Mater. Interfaces* **2019**, *11* (10), 10226−10236.
(31) Chen, W.; Gui, X.; Liang, B.; Yang, R.; Zheng, Y.; Zhao, C.; Li, X.; Zhu, H.; Tang, Z. Structural Engineering for High Sensitivity, Ultrathin Pressure Sensors Based on Wrinkled Graphene and Anodic Aluminum Oxide Membrane. *ACS Appl. Mater. Interfaces* **2017**, *9* (28), 24111−24117.

https://doi.org/10.1021/acsami.3c01175
ACS Appl. Mater. Interfaces 2023, 15, 13813−13821

(32) Huang, C. B.; Witomska, S.; Aliprandi, A.; Stoeckel, M. A.; Bonini, M.; Ciesielski, A.; Samori, P. Molecule-Graphene Hybrid Materials with Tunable Mechanoresponse: Highly Sensitive Pressure Sensors for Health Monitoring. *Adv. Mater.* **2019**, *31* (1), 1804600.
(33) Zhan, Z.; Lin, R.; Tran, V. T.; An, J.; Wei, Y.; Du, H.; Tran, T.; Lu, W. Paper/Carbon Nanotube-Based Wearable Pressure Sensor for Physiological Signal Acquisition and Soft Robotic Skin. *ACS Appl. Mater. Interfaces* **2017**, *9* (43), 37921−37928.
(34) Wan, S.; Bi, H.; Zhou, Y.; Xie, X.; Su, S.; Yin, K.; Sun, L. Graphene Oxide as High-Performance Dielectric Materials for Capacitive Pressure Sensors. *Carbon* **2017**, *114*, 209−216.
(35) Tewari, A.; Gandla, S.; Bohm, S.; McNeill, C. R.; Gupta, D. Highly Exfoliated MWNT-rGO Ink-Wrapped Polyurethane Foam for Piezoresistive Pressure Sensor Applications. *ACS Appl. Mater. Interfaces* **2018**, *10* (6), 5185−5195.
(36) Ma, Y.; Li, Z.; Han, J.; Li, L.; Wang, M.; Tong, Z.; Suhr, J.; Xiao, L.; Jia, S.; Chen, X. Vertical Graphene Canal Mesh for Strain Sensing with a Supereminent Resolution. *ACS Appl. Mater. Interfaces* **2022**, *14* (28), 32387−32394.
(37) Ruth, S. R. A.; Feig, V. R.; Tran, H.; Bao, Z. Microengineering Pressure Sensor Active Layers for Improved Performance. *Adv. Funct. Mater.* **2020**, *30* (39), 2003491.
(38) Zheng, Q.; Lee, J.-h.; Shen, X.; Chen, X.; Kim, J.-K. Graphene-Based Wearable Piezoresistive Physical Sensors. *Mater. Today* **2020**, *36*, 158−179.
(39) Kang, K.; Park, J.; Kim, K.; Yu, K. J. Recent Developments of Emerging Inorganic, Metal and Carbon-Based Nanomaterials for Pressure Sensors and Their Healthcare Monitoring Applications. *Nano Res.* **2021**, *14* (9), 3096−3111.
(40) Liu, M.; Pu, X.; Jiang, C.; Liu, T.; Huang, X.; Chen, L.; Du, C.; Sun, J.; Hu, W.; Wang, Z. L. Large-Area All-Textile Pressure Sensors for Monitoring Human Motion and Physiological Signals. *Adv. Mater.* **2017**, *29* (41), 1703700.
(41) Han, J.; Ma, Y.; Wang, M.; Li, L.; Tong, Z.; Xiao, L.; Jia, S.; Chen, X. Oxygen-Assisted Trimming Growth of Ultrahigh Vertical Graphene Films in a PECVD Process for Superior Energy Storage. *ACS Appl. Mater. Interfaces* **2021**, *13* (10), 12400−12407.
(42) Ma, Y.; Jiang, W.; Han, J.; Tong, Z.; Wang, M.; Suhr, J.; Chen, X.; Xiao, L.; Jia, S.; Chae, H. Experimental Investigation on Vertically Oriented Graphene Grown in a Plasma-Enhanced Chemical Vapor Deposition Process. *ACS Appl. Mater. Interfaces* **2019**, *11* (10), 10237−10243.
(43) Chao, M.; He, L.; Gong, M.; Li, N.; Li, X.; Peng, L.; Shi, F.; Zhang, L.; Wan, P. Breathable Ti3C2Tx MXene/Protein Nanocomposites for Ultrasensitive Medical Pressure Sensor with Degradability in Solvents. *ACS Nano* **2021**, *15* (6), 9746−9758.
(44) Jung, Y.; Choi, J.; Lee, W. J.; Ko, J. S.; Park, I.; Cho, H. Irregular Microdome Structure-Based Sensitive Pressure Sensor Using Internal Popping of Microspheres. *Adv. Funct. Mater.* **2022**, *32* (27), 2201147.
(45) Li, Y.; Cui, Y.; Zhang, M.; Li, X.-d.; Li, R.; Si, W.; Sun, Q.; Yu, L.-m.; Huang, C. Ultrasensitive Pressure Sensor Sponge Using Liquid Metal Modulated Nitrogen-Doped Graphene Nanosheets. *Nano Lett.* **2022**, *22* (7), 2817−2825.
(46) Wu, S.; Yang, C.; Hu, J.; Pan, M.; Qiu, W.; Guo, Y.; Sun, K.; Xu, Y.; Li, P.; Peng, J.; Zhang, Q. Wide-Range Linear Iontronic Pressure Sensor with Two-Scale Random Microstructured Film for Underwater Detection. *ACS Omega* **2022**, *7* (48), 43923−43933.
(47) Xie, Y.; Cheng, Y.; Ma, Y.; Wang, J.; Zou, J.; Wu, H.; Yue, Y.; Li, B.; Gao, Y.; Zhang, X.; Nan, C. W. 3D MXene-Based Flexible Network for High-Performance Pressure Sensor with a Wide Temperature Range. *Adv. Sci.* **2022**, 2205303.
(48) Su, E.; Wu, F.; Zhao, S.; Li, Y.; Deng, C. Layered MXene/Aramid Composite Film for a Soft and Sensitive Pressure Sensor. *ACS Appl. Mater. Interfaces* **2022**, *14* (13), 15849−15858.
(49) Li, A.; Cui, C.; Wang, W.; Zhang, Y.; Zhai, J.; Guo, R.; Cheng, C.; Qin, W.; Ren, E.; Xiao, H.; Zhou, M.; Zhang, J. Compressible and Sensitive Aerogels Derived from Graphene/Waste Paper for Wearable Pressure Sensor. *J. Mater. Sci. Mater. Electron.* **2022**, *33*, 4388−4399.
(50) Long, Z.; Liu, X.; Xu, J.; Huang, Y.; Wang, Z. High-Sensitivity Flexible Piezoresistive Pressure Sensor Using PDMS/MWNTS Nanocomposite Membrane Reinforced with Isopropanol for Pulse Detection. *Sensors* **2022**, *22* (13), 4765.
(51) Duan, Y.; Wu, J.; He, S.; Su, B.; Li, Z.; Wang, Y. Bioinspired Spinosum Capacitive Pressure Sensor Based on CNT/PDMS Nanocomposites for Broad Range and High Sensitivity. *Nanomaterials* **2022**, *12*, 3265.
(52) Park, S.-J.; Kim, J.; Chu, M.; Khine, M. Flexible Piezoresistive Pressure Sensor Using Wrinkled Carbon Nanotube Thin Films for Human Physiological Signals. *Adv. Mater. Technol.* **2018**, *3*, 1700158.
(53) Zheng, W.; Xu, H.; Wang, M.; Duan, Q.; Yuan, Y.; Wang, W.; Gao, L. On-Skin Flexible Pressure Sensor with High Sensitivity for Portable Pulse Monitoring. *Micromachines* **2022**, *13* (9), 1390.
(54) Zhang, X.; Lu, L.; Zhang, P.; Liu, J.; Yang, B. A Durable Flexible Pressure Sensor with High Sensitivity and Wide Pressure Range for Health Monitoring. *Proceedings of the IEEE 35th International Conference on Micro Electro Mechanical Systems Conference (MEMS)*; Tokyo, Japan, Jan 9−13, 2022; pp 333−336, DOI: 10.1109/MEMS51670.2022.9699763.
(55) Xu, J.; Li, H.; Yin, Y.; Li, X.; Cao, J. W.; Feng, H. F.; Bao, W.; Tan, H.; Xiao, F.; Zhu, G. High Sensitivity and Broad Linearity Range Pressure Sensor Based on Hierarchical In-Situ Filling Porous Structure. *npj Flexible Electron.* **2022**, *6*, 1−12.
(56) Yin, Y.; Li, H. Y.; Xu, J.; Zhang, C.; Liang, F.; Li, X.; Jiang, Y.; Cao, J. W.; Feng, H. F.; Mao, J. N.; Qin, L.; Kang, Y. F.; Zhu, G. Facile Fabrication of Flexible Pressure Sensor with Programmable Lattice Structure. *ACS Appl. Mater. Interfaces* **2021**, *13* (8), 10388−10396.
(57) Zhao, T.; Yuan, L.; Li, T.; Chen, L.; Li, X.; Zhang, J. Pollen-Shaped Hierarchical Structure for Pressure Sensors with High Sensitivity in an Ultrabroad Linear Response Range. *ACS Appl. Mater. Interfaces* **2020**, *12* (49), 55362−55371.
(58) Wang, S.; Zhang, Z.; Yang, B.; Zhang, X.; Shang, H.; Jiang, L.; Liu, H.; Zhang, J.; Hu, P. High Sensitivity Tactile Sensors with Ultrabroad Linear Range Based on Gradient Hybrid Structure for Gesture Recognition and Precise Grasping. *Chem. Eng. J.* **2023**, *457*, 141136.
(59) Wang, J.; Zhong, Y.; Dai, S.; Zhu, H.; Wu, L.; Gu, F.; Cheng, G.; Ding, J. Ag Nanowire/CPDMS Dual Conductive Layer Dome-Based Flexible Pressure Sensor with High Sensitivity and a Wide Linear Range. *ACS Appl. Nano Mater.* **2022**, *5* (9), 13227−13235.
(60) Luo, R.; Cui, Y.; Li, H.; Wu, Y.; Du, B.; Zhou, S. A Sponge-Like High Sensitivity Wearable Piezoresistive Pressure Sensor Based on Fragmented Graphene Aerogel/ Polydimethylsiloxane. *SSRN Electron. J.* **2022**, 4138054.